e-Polymers **2002**, no. 036. http://www.e-polymers.org

Low voltage scanning electron microscopy and atomic force microscopy: state-of-the-art microscopy techniques for investigations of polymer single crystals

*Joachim Loos** , *Mingwen Tian*

Eindhoven Polymer Laboratories, Dutch Polymer Institute, Eindhoven University of Technology, 5600 MB Eindhoven, The Netherlands; Fax +31-40-243 6999; j.loos@tue.nl

(Received: May 28, 2002; published: August 15, 2002)

Abstract: Recent studies on organization and reorganization of polymer single crystals have contributed to the actual discussion on novel approaches towards understanding polymer crystallization and melting. In this context, low voltage scanning electron microscopy (LVSEM) and atomic force microscopy (AFM) demonstrate their importance for the investigation of polymer crystals. Both techniques are able to visualize the morphology of individual single crystals, which have a thickness in the order of 10 to 30 nm and a lateral size of a few micrometers, respectively, without any additional sample treatment such as coating or etching. Main advantage of LVSEM is its large range of observation: LVSEM is suited for fast screening and sample quality evaluation on the millimeter or micrometer level, and at the same time it has the prospect for detection of morphological details with nanometer resolution. The main strength of AFM is twofold: first, its excellent ability for precise quantitative thickness determination of the crystals, and second, using non-contact mode it can act as a non-destructive investigation technique, which allows *in situ* investigation of dynamic processes during sample treatment. By presenting some results of our studies, e.g., time dependent growth or temperature dependent annealing behavior of individual single crystals, we like to point out the specific advantages of the two techniques for fundamental studies on individual crystals, or ultra-thin polymer layers in general.

Introduction

The study of crystalline morphology in polymer systems aims at understanding the various levels of organization as well as their temporal development. Investigation of single crystals has been performed and still plays an important role in determining and understanding the crystallization mechanism of polymer materials [1-5]. Polyethylene and other linear polymers crystallize from dilute solution as folded chain single crystals in the form of thin platelets [6-8]. Polymer chains in such crystals run almost perpendicular to the lamellar plane and fold back upon themselves more or less adjacent to the lamellar surfaces. The thickness of the platelets, which is typically in the order of 10 to 30 nm, increases with the crystallization temperature.

Standard investigation techniques such as small angle X-ray scattering (SAXS), Raman spectroscopy or transmission electron microscopy (TEM), have proven their strength to analyze the structure of single crystals [9-16]. Using single crystal mats consisting of millions of individual crystals, SAXS and Raman spectroscopy are able

to determine, e.g., the average thickness of the crystals or the stem length incorporated in the crystals, respectively. Also, these techniques are able to follow structural changes of the crystals during, e.g., temperature or time dependent experiments. On the other hand, TEM is the most powerful technique to visualize in detail the morphology (lateral size, shape) of individual crystals and to gain local structural information by means of electron diffraction. The main drawback of TEM is the sample damage caused by interaction of the primary electron beam with the polymer crystal.

As a conclusion, standard investigation techniques are very helpful tools for the determination of structure and morphology of single crystals, but these techniques are not able to follow *dynamic* changes of *individual* single crystals during, e.g., annealing experiments. Therefore, local or temporary variations from the average morphology and structure evolution of individual crystal species are less or even not identified. However, there are indications that on a nanometer scale (measured by atomic force microscopy (AFM) [17]), e.g., growing rates of polyethylene lamellae significantly differ from growing rates determined by, e.g., optical microscopy (micrometer resolution) or differential scanning calorimetry (average values). Thus, it is the purpose of the present study to introduce two state-of-the-art microscopy techniques, namely low voltage scanning electron microscopy (LVSEM) and AFM, for direct visualization of individual polymer single crystals with nanometer resolution. Also, it will be demonstrated that the combination of LVSEM and AFM offers distinct advantages over conventional techniques for investigation of dynamic organization and reorganization processes of polymer single crystals.

Results and discussion

The development of LVSEM techniques has been driven by practical applications, initially in the semiconductor industry, based on the very different characteristics of electron beam/specimen interaction at low voltages, i.e., of acceleration voltages $E_0 \approx 1$ keV, and despite the reduced performance of electron microscope columns under these conditions. Most important for the investigation of non-conducting materials such as polymers is the ability to produce quality images at low accelerating beam voltages, which minimizes beam damage to the sample [18] and affords an operating window where the sample does not build up negative charge. At sufficiently low voltages, total electron yield may reach unity, which may give enhanced contrast and high resolution in the case of non-conductive samples. This obviates the normal requirement to coat samples with a conductive layer. Moreover, the penetration depth of primary electrons in polymers (mainly carbon) is in the order of a few 10 nm for low acceleration voltages. Therefore, one consequence is that relatively more secondary electrons are generated close enough to the surface to escape from the interesting sample, which may increase the signal to noise ratio.

To minimize charging and its associated problems, incident beam energy must be carefully chosen to be the so-called value E_2 at which the dynamic charge balance is obtained. Primary electron energies above E_2 result for insulating materials in localized negative charge assembly, which drastically reduces or even obstructs image quality. For electron incident at energies below E_2, and horizontal and flat samples, the electron yield is greater than unity. In a conductor, the excess electrons required for charge balance are drawn from ground as specimen current. For an insulator, positive charging will occur, but because the positive potential leads to recollection of secondary electrons emitted from the sample, the extent of the charge is limited.

Data of E_2 for different materials can be measured using SEM at various accelerating voltages or can be calculated mainly by means of Monte Carlo modeling [19-22]. Typical E_2 values are: carbon ≈ 0.7 keV, silicon oxide ≈ 2 - 3 keV, gold ≈ 6 - 8 keV, respectively. Therefore, the choice of appropriate primary electron energy prior to observation can minimize the possible irreversible build up of charge-related artifacts.

The use of low electron acceleration voltages results in short penetration depths of the primary electrons in the samples, which turn out to be, in the present case, an even more distinct advantage. The enhancement in surface sensitivity is due to the significant decrease in the electron range by decreasing the incident beam energy [23,24]. This can be demonstrated by using either the Kanaya-Okayama range calculations or Monte Carlo simulation routines. The Kanaya-Okayama range is given by

$$R_{KO} = 2.76 \times 10^{-11} A E_0^{1.67} / (Z^{0.889} \times d)\, cm \qquad (1)$$

where E_0 is the incident electron energy (in keV), A the average atomic weight (in g), d the density of the material (in g/cm^3), and Z the atomic number of the target. Although the calculation at energies less than 5 keV is somewhat questionable, previously published work shows that at energies in the range of 0.5 keV to 2 keV, the electron range is only in the order of tens of nanometers for polymers [24].

Similar penetration depths of the primary electrons can be calculated using Monte Carlo simulations. For incident electron beam energy of 20 keV, as used for conventional investigation, the electron range in a carbon target is in the order of 2 µm; for beam energy of 1 keV, the electron range in carbon is reduced to approximately 20 nm. In the case of a gold target, the electron range for 20 keV is 0.5 µm and for 1 keV shorter than 10 nm, respectively.

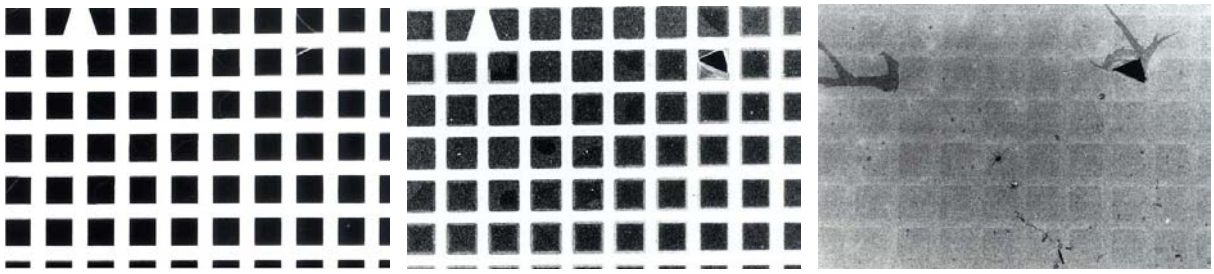

(a) (b) (c)

Fig. 1. Set of LVSEM images of a 10 nm thin gold film evaporated on a copper grid coated with an ultra-thin carbon film; secondary electron detector and different acceleration voltages are used: (a) 20 keV; (b) 5 keV; and (c) 1 keV. The contrast enhancement of the thin gold layer can be followed best by observation of the hole located at the right top of the sample

To demonstrate the influence of the incident beam energy on surface sensitivity of the LVSEM technique, we have performed the following experiment: a 10 nm thin gold film was evaporated on a copper grid coated with an ultra-thin carbon film and subsequently imaged changing the acceleration voltage from 20 keV to 1 keV. Fig. 1 shows LVSEM images of this sample. For the highest acceleration voltage only the copper grid can be imaged (Fig. 1a). Additional sample features become visible by lowering the acceleration voltage: a thin film seems to cover the holes of the copper grid (Fig. 1b). For a beam energy of 1 keV the copper grid is hardly visible; the gold layer dominates the contrast formation of the image (Fig. 1c). Contrast enhancement

of the gold layer through the accelerating voltage set can be followed best by observation of the hole in the coating layer located right top of the sample.

In the case of polyethylene single crystals, we are dealing with specimens that have a thickness in the order of 10 nm, a lateral size of a few micrometers, and consist of carbon and hydrogen. Adjusting the LVSEM to an acceleration voltage of 700 eV eliminates charging and minimizes beam damage. Fig. 2a shows a low magnification image of isolated or agglomerated polyethylene single crystals deposited on a mica substrate. At this magnification, high-speed screening of number and quality of the single crystals can be performed. At the same time, higher magnification results in detailed morphological information with semi-high resolution. In Fig. 2b, several common features of polyethylene single crystals grown from solution can be observed: the central nucleus formed during the self-seeding procedure; the lozenge shape; and dominant corrugation lines formed due to sedimentation of the crystal on the mica substrate. Fig. 2c shows two crystals stacked together. Focusing our interest to the area of the image where the crystals overlap, a distinct contrast between single and double layers can be seen. In the present case, the thickness of a single layer is in the order of 12 nm, and the double layer has a thickness of about 24 nm. Thus, using LVSEM qualitative thickness determination with nanometer resolution can be performed. Details on the contrast mechanism may be found in ref. [25].

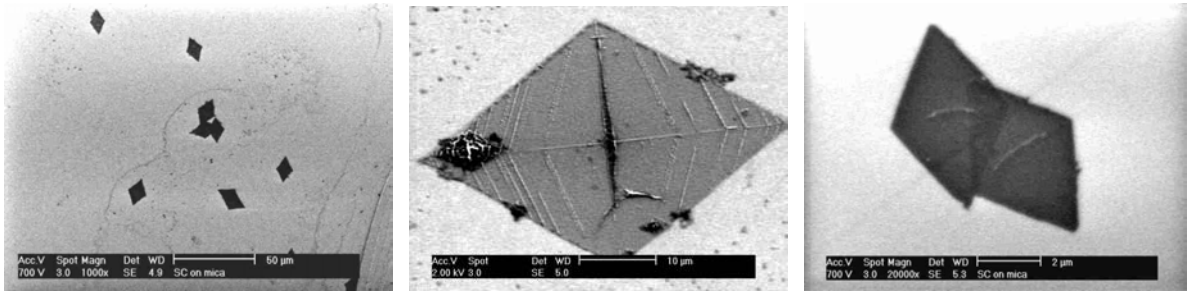

(a) (b) (c)

Fig. 2. Set of LVSEM images of solution grown polyethylene single crystals; secondary electron detector is used: (a) low magnification image of isolated or agglomerated polyethylene single crystals deposited on a mica substrate; (b) individual single crystal with central seed and pronounced corrugation lines; and (c) crystals showing a distinct height contrast in the stacked area in the center of the image

As a first summary, using LVSEM visualization of polymer single crystals is possible. LVSEM is a powerful tool for high-speed evaluation of sample quality, and it is able to characterize morphological features of polymer single crystals in detail with semi-high resolution. However, it is not possible to follow dynamic processes using LVSEM, because sample damage caused by the electron beam during observation, even at very low acceleration energies, cannot be prevented.

As stated in the Introduction, there are indications that on a local, nanometer scale morphology and structure evolution during experimental treatments of polymer crystals may differ significantly from their average behavior as observed by scattering or spectroscopic techniques. Thus, non-destructive investigation techniques having nanometer resolution and being able to visualize morphological and structural features of individual crystals may help understanding local dynamic organization and reorganization processes of polymer crystals.

AFM fulfils these demands. Since the development of AFM, studies have been aimed at visualization of morphology, nanostructure, and molecular order and have been performed on a large number of different polymer samples. Moreover, AFM can measure directly lateral sizes as well as the thickness of crystals.

Main advantage of AFM, in the present case, is its ability to image samples using non-contact modes, which do not destroy or even interfere with soft polymer materials [17,26]. In conventional contact AFM, the probe tip is simply dragged across the surface and the resulting image is a topographical map of the sample surface. Because of the strong sample-tip interaction contact, AFM provides highest resolution. On the other hand, the dragging motion of the probe tip, combined with friction, adhesive or electrostatic forces between the tip and the surface, may cause substantial damage of the sample, especially in the case of soft matter samples.

Non-contact modes using oscillating probe tips overcome the limitations of the conventional contact mode, because the tip alternately is placed in contact with the sample surface to provide high resolution and than is lifted off the surface to avoid dragging the tip across the surface. Common tip cantilever oscillation frequencies are in the order of 10 kHz to 500 kHz. At these frequencies, many surfaces become stiff (viscoelastic) and can more easily resist forces from the probe tip. This property further reduces the possibility of sample damage for extremely soft samples such as polymers and biological specimens and causes less distortion of the sample surface due to tip forces.

Tab. 1. Crystallization temperature (T_c) and initial lamellae thickness (L, L_C corrected) of several single crystal species. For calculation of the corrected lamellae thickness we assume a total thickness of the amorphous layer of 0.8 nm, which is subtracted from the measured lamellae thickness. The shapes of the crystals were lozenge or truncated lozenge

T_C in ºC	L / nm	L_C / nm
75	10.5	9.7
78	11.4	10.6
80	11.7	10.9
85	12.3	11.5
86	13.1	12.3
88	14.5	13.7
95	17.3	16.5

In the present study we have used AFM in non-contact imaging mode for observations of the shapes and sizes of polyethylene single crystals, for exact measurements of crystal thickness and for investigations of dynamic morphology changes of the crystals during annealing, melting and recrystallization experiments. The thickness of polyethylene (PE) single crystals prepared from dilute solution depends on the crystallization temperature: with increasing temperature the lamellae become thicker. From the AFM data, both the real thickness and the surface roughness of the single crystals can be determined. Using different sections of one individual single

crystal, it is observed that the thickness is uniform through the whole lamella with a deviation of $\pm$ 0.2 nm, which corresponds to surface roughness. Lamellar thickness measured for different crystallization temperatures is summarized in Tab. 1. AFM height data of single crystals represent always the core crystal thickness (L_C) together with the amorphous layers coated on both sides. Our thickness data scatter in the order of $\pm$ 0.4 nm and are calculated on the basis of measurements of several crystals grown from different solution batches. Taking the error range into account, our data match with the well established and often confirmed SAXS data, e.g., of Mandelkern et al. [27]. Thus, thickness measurement of PE single crystals using AFM must be considered as accurate.

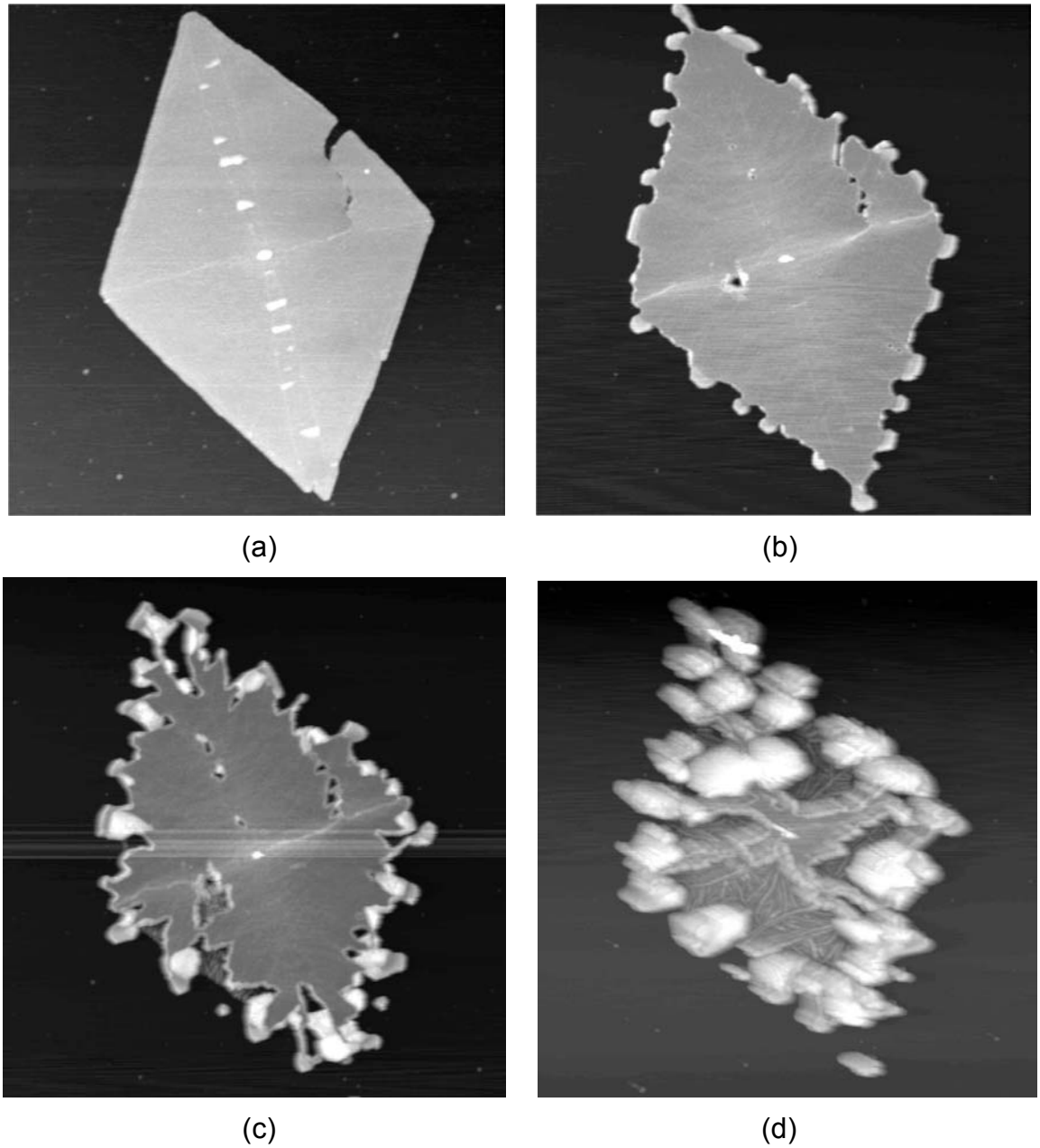

Fig. 3. AFM images in height contrast mode of an individual solution grown single crystal at different annealing temperatures: (a) room temperature, initial crystal; (b) T_{ann} = 110ºC; (c) T_{ann} = 120ºC; and (d) T_{ann} = 138ºC, and cooled to room temperature. The size of the images is 9 x 9 µm

A typical sequence of AFM images in height contrast mode corresponding to the evolution of one individual single crystal during an annealing experiment is presented in Fig. 3. The single crystal is originally grown at 85ºC in xylene, has an overall thickness of ≈ 12.3 nm and a slightly truncated shape (Fig. 3a). Distinct changes of the truncated single crystal appearance are visible at elevated annealing temperatures (Fig. 3b): reorganization, possibly melting and recrystallization, starts from the initial edges of the crystal and from some defects located within the body of the crystal, and results in a roughening of the crystal shape and the formation of a pronounced rim that has an elevated thickness compared with the original lamella thickness. Further increasing the annealing temperature, the reorganization of the crystal continues (Fig. 3c). In addition to the rim formation at the crystal edges, also a partial reorganization of the two {200} sectors is detectible. Finally, annealing above its melting temperature results in complete melting of the single crystal. After subsequent cooling to room temperature, the polyethylene recrystallizes and forms edge-on and flat-on lamellar crystals (Fig. 3d). Even after this annealing and cooling procedure, the just formed melt crystallized lamellae are located only in the area where the initial solution grown single crystal had been placed. More details of the reorganization of solution grown polyethylene single crystals will be introduced and discussed elsewhere.

Experimental part

The material used in this study was kindly provided by Phillips Petroleum Comp., USA (linear PE with M_w ≈ 100 kg/mol, M_w/M_n ≈ 1.04). Individual single crystals were prepared by isothermal crystallization of dilute solutions of PE in xylene (≈ 0.01 wt.-%) at various temperatures. To insure fairly uniform crystal size and shape, the technique of self-nucleation was followed [28]. Single crystals were removed from the solution at different times of crystallization (minutes to days and weeks) by simply dipping freshly cleaved mica or small silicon wafer pieces into the solution followed by subsequent drying the samples in a vacuum oven at 40°C for 24 h. Some of the samples were annealed after deposition on the substrates.

Morphological investigation of the as prepared polyethylene single crystals was performed using a Philips environmental scanning electron microscope XL30 ESEM-FEG, which is equipped with a field emission electron source, using low voltage mode and a secondary electron detector.

In situ AFM investigations during annealing of the samples were performed using a Smena P47H, NT-MDT Ltd., Moscow, Russia, which is equipped with a heating stage. The AFM was calibrated using height standards produced by Silicon-MDT Ltd., Moscow, Russia.

Acknowledgement: Helpful discussions with Anette Thiery, Marcel Dosière, Stephane Hocquet and Bernard Lotz are appreciated.

[1] Keller, A.; *Philos. Mag.* **1957**, *2*, 1171.

[2] Keller, A.; Toda, A.; *Colloid Polym. Sci.* **1993**, *271*, 328.

[3] Organ, S. J.; Keller, A.; Wills, H. H.; J. *Polym. Sci., Polym. Phys.* **1986**, *24*, 2319.

[4] Armistead, K.; Wood, G. G.; Keller, A.; *Adv. Polym. Sci.* **1992**, *100*, 220.

[5] Lotz, B.; Kovacs, A. J.; Wittmann, J. C.; J. *Polym. Sci., Polym. Phys. Ed.* **1975**, *13*, 909.

[6] Keller, A.; O'Connor, A.; *Nature* **1957**, *180*, 1289.

[7] Keller, A.; O'Connor, A.; *Discuss. Faraday Soc.* **1958**, *25*, 114.

[8] Blundell, D. J.; Keller, A.; Kovacs, A. J.; *J. Polym. Sci.* **1966**, *B4*, 481.

[9] Brown, R. G.; Eby, R. K.; *J. Appl. Phys.* **1964**, *35*, 1156.

[10] Strobl, G. R.; *Kolloid Z. Z. Polym.* **1972**, *250*, 1039.

[11] Martain, V. I. G.; Alamo, R.; Mandelkern, L.; *J. Polym. Sci., Polym. Phys.* **1986**, *24*, 1283.

[12] Schaufele, R. F.; Shimanouchi, T. J.; *Chem. Phys.* **1967**, *47*, 3605.

[13] Koening, J. L.; Tabb, D. L.; *J. Macromol. Sci.* **1974**, *B9*, 141.

[14] Bassett, D. C.; "*Principles of Polymer Morphology*", University Press, Cambridge **1981**.

[15] Martinez-Salazar, J.; Keller, A.; Cagiao, M. E.; Rueda, D. R.; Balta Calleja, F. J.; *Colloid Polym. Sci.* **1983**, *261*, 412.

[16] Matain, V. I. G.; Mandelkern, L.; *J. Polym. Sci., Polym. Phys.* **1989**, *27*, 967.

[17] Hobbs, J. K.; Humphris, A. D. L.; Miles, M. J.; *Macromolecules* **2001**, *34*, 5508.

[18] Price, C. W.; McCarthy, P. C.; *Scanning* **1988**, *10*, 29.

[19] Joy, D. C.; *Scanning* **1989**, *11*, 1.

[20] Joy, D. C; *J. Microsc.* **1987**, *147*, 51.

[21] Ding, Z.-J.; Shimizu, R.; *Scanning* **1996**, *18*, 92.

[22] Cosandey, F.; *Adv. Mater. Processes* **1999**, *7*, 37.

[23] Kanaya, K.; Ohayama, S.; *J. Phys.* **1972**, *D5*, 43.

[24] Seah, M. P.; Dend, W. A.; *Surf. Interface Anal.* **1979**, *1*, 2.

[25] Jiang, H.; Patnik, S. S.; Haaland, P.; Vezie, D. L.; Bunning, T.; Williams, J.; Adams, W.; *Atomic Force Microsc./Scanning Tunneling Microsc.* (Proc. U.S. Army Natick Res., Dev. Eng. Cent. Symp.) **1994**, *1*, 153.

[26] Tian, M.; Loos, J.; *J. Polym. Sci., Polym. Phys.* **2001**, *39*, 763.

[27] Mandelkern, L.; Sharma, R. K.; Jackson, J. F.; *Macromolecules* **1969**, *2*, 644.

[28] Blundell, D. J.; Keller, A.; Kovacs, A. J.; *J. Polym. Sci.* **1966**, *B4*, 481.